Journal of Solid State Chemistry **157,** 1–7 (2001)
doi:10.1006/jssc.2000.9012, available online at http://www.idealibrary.com on IDEAL®

# Crystal Structure of the $Ba_4CeNb_{10}O_{30}$ Reduced Niobate with a TTB-Type Structure

A. V. Mironov, S. Ya. Istomin, O. G. D'yachenko, and E. V. Antipov

*Department of Chemistry, Moscow State University, Leninskie Gory, 119899 Moscow, Russia*

Received March 23, 2000; in revised form October 12, 2000; accepted October 27, 2000

**The structure of the cation-deficient $Ba_{4.0(1)}Ce_{0.98(3)}Nb_{10}O_{30}$ barium cerium reduced niobate with a tetragonal tungsten bronze (TTB) type structure was refined from X-ray single crystal data (tetragonal, $a = 12.508(2)$ Å, $c = 3.9328(4)$ Å, S. G. *P4/mbm*, $Z = 1$, $R = 0.019$, $R_w = 0.023$). It was found that rare earth substitution for Ba is accompanied by formation of vacancies in *A* sites. Vacancies were preferably formed in the *A*(1) cavities in the structure.** © 2001 Academic Press

## INTRODUCTION

The tetragonal tungsten bronze type structure (TTB) is built up of a corner-shared niobium–oxygen octahedra network with three different types of channels in the structure. It can be described by the general formula $(A(1))_2(A(2))_4C_4Nb_{10}O_{30}$, where *A*(1), *A*(2), and *C* are the notations of the different sites in the crystal structure (1). Cations in the *A*(1) cavities have a cuboctahedral coordination by oxygen atoms while in *A*(2) and *C* cavities they have a pentacapped pentagonal prismatic coordination and a tricapped trigonal prismatic coordination, respectively. The size of these cavities decreases in the order $A(2) > A(1) > C$. In the TTB-type compounds alkaline and/or alkaline earth metals are located in the *A*(1) and *A*(2) sites, while in the *C* site small cations such as Li (2) or Nb (3) are found.

Among reduced niobates $A_6Nb_{10}O_{30}$ compounds with the TTB-type structure were obtained for $A$ = Sr, Ba, and Eu (4–7). Nonsubstituted $A_6Nb_{10}O_{30}$ compounds are semiconductors. The probable reason for this is a rather low charge carrier concentration—$0.2\bar{e}$ per Nb atom for $A_6^{2+}Nb_{10}O_{30}$. Recently the influence of the heterovalent substitution of rare earth cations for barium on the crystal structure and conductivity of $Ba_{6-x}Ln_xNb_{10}O_{30}$, $Ln$ = La, Ce, Nd, compounds was studied (6, 7). Such substitution led to the increase of the charge carrier concentration up to $0.4\bar{e}$ per Nb atom for the most substituted sample with the nominal composition $Ba_4La_2Nb_{10}O_{30}$. This value is quite close to that found in $Na_{0.45}W_{10}O_{30}$ ($0.45\bar{e}$ per Nb) with metallic-type conductivity (8). Despite the increase in the number of electrons per Nb atom the temperature dependence of the normalized resistivity for $Ba_{6-x}Ln_xNb_{10}O_{30}$ ($Ln$ = La, Ce, Nd; $0 \le x \le 2$) compounds was nonmetallic in all cases since the slope $\partial\rho/\partial T$ was negative (6, 7). One possible reason for the nonmetallic behavior is likely to be the creation of cation vacancies in the Ba/*Ln* sites, which leads to a decrease in the charge carrier concentration calculated for the stoichiometric composition. Such a possibility was reported for the numerous compounds having TTB-type structure; see for example $Ba_{6-x}Ta_{10}O_{30}$ (9). The structural refinement from X-ray powder data combined with thermogravimetric analysis in oxygen and EDS analysis confirmed the existence of the vacancies in the *A* network for $Ba_{6-x}Ln_xNb_{10}O_{30}$ ($Ln$ = La, Ce, Nd; $0 \le x \le 2$) (7). However, X-ray powder data should be used carefully for the refinement of atomic occupancies due to the correlation effect between these parameters and thermal ones.

The aim of the present work was the single crystal preparation of rare earth substituted reduced niobates with TTB-type structure and the study of cation vacancy distribution in Ba and *Ln* sites.

## EXPERIMENTAL

The single crystals of $Ba_{6-x}Ln_xNb_{10}O_{30}$ were grown by the method described by Hessen *et al.* (4) with minor modifications. Starting materials were $Ba_{6-x}Ln_xNb_{10}O_{30}$ ($Ln$ = La, Ce, Nd; $0 \le x \le 2.5$) powder samples and a borate flux of $BaO \times 1.79B_2O_3$ composition. The powder samples were prepared by heating pellets of intimately mixed stoichiometric amounts of $NbO_2$, $Nb_2O_5$, $Ba_5Nb_4O_{15}$, and $Ln_2O_3$ ($CeO_2$) in evacuated and sealed silica tubes at 1200–1250°C for 10–48 h. The $BaO \times 1.79B_2O_3$ flux ($T_m = 889$°C) was synthesized by heating the stoichiometric mixture of $B_2O_3$ (99.999) and $Ba(NO_3)_2$ (99.999) in air at 750°C for 48 h.

Initial reagents ($Ba_{6-x}Ln_xNb_{10}O_{30}$ and $BaO \times 1.79B_2O_3$) were mixed in a 1:3 mass ratio, placed in alumina crucibles, and sealed in evacuated silica tubes. The mixture was heated at 1050°C for 3 h. Then it was cooled at



0022-4596/01 $35.00

a rate of 6°C/h down to 850°C and then the furnace was cooled automatically to room temperature. The glassy flux was removed by etching with a dilute aqueous HF solution.

The best single crystals were obtained for Ce-substituted compound with nominal composition $Ba_{3.5}Ce_{2.5}Nb_{10}O_{30}$. Black pillar-shaped crystals were selected from this sample and investigated. Unit cell dimensions were determined by least squares from 24 reflections in the range $15° \leq \Theta \leq 16°$. No superstructure was found by electron diffraction on the ceramic samples of $Ba_{6-x}Ln_xNb_{10}O_{30}$ ($Ln$ = La, Ce, Nd; $0 \leq x \leq 2.5$) (7). The cation composition of the crystal was analyzed at eight points with the CAMEBAX-microBEAM instrument. Atomic percentages were determined using the $L\alpha$ lines of Nb, Ba, and Ce. $Ba_6Nb_{10}O_{30}$ and $CeO_2$ were used as standards. The MBX COR program (ZAF-correction) was used for the calculations. Normalized for 10 Nb atoms the composition of the crystal was determined to be $Ba_{4.0(1)}Ce_{0.98(3)}Nb_{10}O_{30}$. The crystal structure was refined by the JANA98 program package (10).

The description and results of the single crystal experiment are given in Table 1. All stages of the refinement are briefly described in Table 2.

**TABLE 1**
**Summary of Crystallographic Information for $Ba_4CeNb_{10}O_{30}$**

| | |
|---|---|
| Crystal data | |
| Chemical formula | $(Ba, Ce)_{5.16}Nb_{10}O_{30}$ |
| Molecular weight | 2120.65 |
| Crystal system | Tetragonal |
| Space group | $P4/mbm$ |
| Cell constants (Å) | $a = 12.508(2)$ $c = 3.9328(4)$ |
| Volume (Å$^3$) | 615.3(1) |
| $Z$ | 1 |
| $D_{calc}$ (g cm$^{-3}$) | 5.721 |
| Radiation | Mo$K\alpha$ |
| Wavelength (Å) | 0.71073 |
| No. of reflections for cell parameters determination | 24 |
| $\theta$ range (°) | 15–16 |
| Linear absorption coefficient (cm$^{-1}$) | 127.89 |
| Temperature (K) | 293 |
| Crystal form | Column |
| Crystal size (mm) | $0.74 \times 0.12 \times 0.055$ |
| Color | Black |
| Data collection | |
| Diffractometer | CAD4, Graphite monochromator |
| Data collection method | $\omega$-1.33$\theta$ scans |
| Absorption correction | Analytical (crystal shape) |
| No. of measured reflection | 3135 |
| No. of independent reflection | 720 |
| No. of observed reflection | 622 |
| Criteria for observed reflections | $I > 3\sigma(I)$ |
| $\theta$ limits (°) | 2–35 |
| Range of $h$, $k$, $l$ | $-20 \rightarrow h \rightarrow 20$<br>$0 \rightarrow k \rightarrow 20$<br>$0 \rightarrow l \rightarrow 6$ |
| $R_{int}$ | 0.017 |
| No. of standard reflections for intensity correction | 1 |
| Frequency of standard reflections (min) | 120 |
| Intensity decay (%) | $\leq 1.93$ |
| Refinement | |
| Refinement on | $F$ |
| $R/R_w$ ($I > 3\sigma(I)$) | 0.019/0.023 |
| Goodness of fit | 0.92 |
| No. of reflections used in refinement | 622 |
| No. of refined parameters | 54 |
| Weighing scheme | $w = \sigma^{-2}(F)$ |
| $(\Delta/\sigma)_{max}$ | 0.0002 |
| $\Delta r_{max}$ (e Å$^{-3}$) positive/negative | 1.24/ − 1.40 |

## RESULTS AND DISCUSSION

Starting parameters for the refinement were taken from a paper by Hessen *et al.* (4). As it is impossible to distinguish by X-rays Ce and Ba, the $A(1)$ and $A(2)$ sites were set to be occupied by only one type of atom each, because no way to estimate the amount of each cation in these sites was found. Nevertheless the real joint occupancy refinement of these sites by both types of atoms should lead to essentially the same result as their $f$ curves are similar. Thus the $A(1)$ site was set to be occupied by Ce while the $A2$ site was set to be occupied by Ba. It is well-known that the largest cavities $A(2)$ in the TTB-type structure are preferably occupied by the largest atoms while the $A(1)$ sites are occupied by the smallest ones. For example, in the $Ba_{2/3}Sr_{1/3}Nb_2O_6$ structure Ba atoms are preferably placed in $A(2)$ sites while Sr atoms are in $A(1)$ sites (11).

At the beginning the occupancies of all sites were set to 1.0. The structure was refined with isotropic atomic displacement parameters (ADP) down to $R = 0.118$ and $R_w = 0.151$. It should be mentioned that high ADP were obtained for $A(2)$ and all oxygen atoms. The refinement with anisotropic ADP for all atoms reduced agreement factors significantly to $R = 0.062$ and $R_w = 0.091$. However, the ADP for the oxygen atoms O(2) and O(5) were negative. Extinction refinement resulted in a small decrease in the $R$ factor (by 0.002) with extinction parameter about $2\sigma$. Thus at this stage extinction parameters were not taken into consideration.

Difference Fourier synthesis showed the negative residual peak at the $A(1)$ site (Fig. 1a). Fourier mapping definitely showed excess of Ce in that position in the model, and thus $A(1)$ site occupancy was refined. The obtained value was 0.743(2). The refinement led to a decrease in the $R$ factors down to $R = 0.028$ and $R_w = 0.036$; reduction of the absolute value of residual peaks (Fig. 1b) and positive ADP for oxygen atoms O(2) and O(5) were obtained.

Next difference Fourier synthesis showed the highest residual peaks around the $A(2)$ site and the Fourier map

**TABLE 2**
**The Comparison of the Results for the Structure Refinement of $Ba_4CeNb_{10}O_{30}$ at Different Stages**

| No. | Parameter | $R$ | $R_w$ | $S$ | Residual peaks (e/Å$^3$) (positive/negative) | Number of parameters | $R/R_0$ | Hamilton $\alpha = 0.01$ |
|---|---|---|---|---|---|---|---|---|
| 1 | Isotropic ADP | 0.118 | 0.151 | 5.83 | 29.3/15.3 | 20 | — | — |
| 2 | Anisotropic ADP | 0.062 | 0.091 | 3.58 | 5.18/10.54 | 41 | 1.903 | 1.032 |
| 3 | $A(1)$ occupancy | 0.028 | 0.036 | 1.43 | 1.68/4.21 | 42 | 2.214 | 1.006 |
| 4 | $A(2)$ occupancy | 0.024 | 0.028 | 1.10 | 2.11/2.93 | 43 | 1.167 | 1.006 |
| 5 | Anharmonic ADP, 4 terms | 0.023 | 0.031 | 1.22 | 1.55/1.74 | 50 | 1.217 | 1.019[a] |
| 6 | Anharmonic ADP, 6 terms | 0.021 | 0.028 | 1.14 | 1.28/1.40 | 57 | 1.095 | 1.022[b] |
| 7 | Final | 0.019 | 0.023 | 0.92 | 1.24/1.40 | 51 | 1.211 | 1.006[b] |
| 8 | Isotropic extinction | 0.018 | 0.023 | 0.90 | 1.29/1.41 | 52 | 1.056 | 1.006[c] |

[a]Compared to $A(1)$ occupancy refinement (3).
[b]Compared to anharmonic ADP refinement (4 terms) (5).
[c]Compared to final refinement (7).

looked complicated (Fig. 2a). Negative density in the $A(2)$ site may result from cation deficiency. At this stage the refinement of the occupancy resulted in a small Ba deficiency ($g(A(2)) = 0.932(4)$) with a decrease in agreement factors down to $R = 0.024$ and $R_w = 0.028$. Difference Fourier synthesis after occupancy refinement showed maximal heights of positive and negative peaks about $\frac{3}{4}$ of that obtained before $A(2)$ occupancy refinement.

Difference Fourier mapping showed asymmetric alteration of positive and negative regions at the $A(2)$ site (Fig. 2b). Besides the distribution of $R$ factors over $\sin\theta/\lambda$, after $A(2)$ occupancy refinement had large variation. It increased from 0.019 for $\sin\theta/\lambda < 0.36$ to 0.044 for $0.76 < \sin\theta/\lambda < 0.81$, which may be the result of inadequate displacement description rather than thermal diffused scattering, which is usually insignificant at these values of $\sin\theta/\lambda$ for structures with such compositions at these temperatures. Taking into account the large size of the channel and the significant difference in Ba and Ce radii (about 0.4 Å) the splitting of the $A(2)$ site into two different atomic positions may be suggested. Such supposition can be represented in the refinement either by two atomic sites about 0.2–0.4 Å

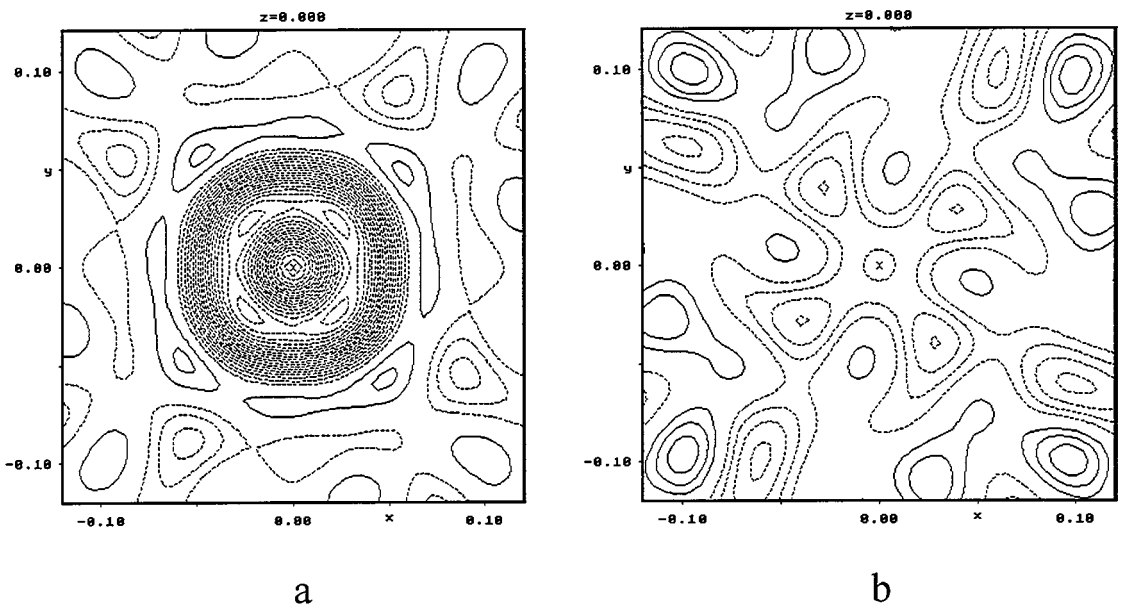


**FIG. 1.** Difference electron density map at $A(1)$ site (negative density is shown as dashed lines): (a) before occupancy refinement; (contour interval at 0.5 e/Å$^3$); (b) after occupancy refinement (contour interval at 0.2 e/Å$^3$).

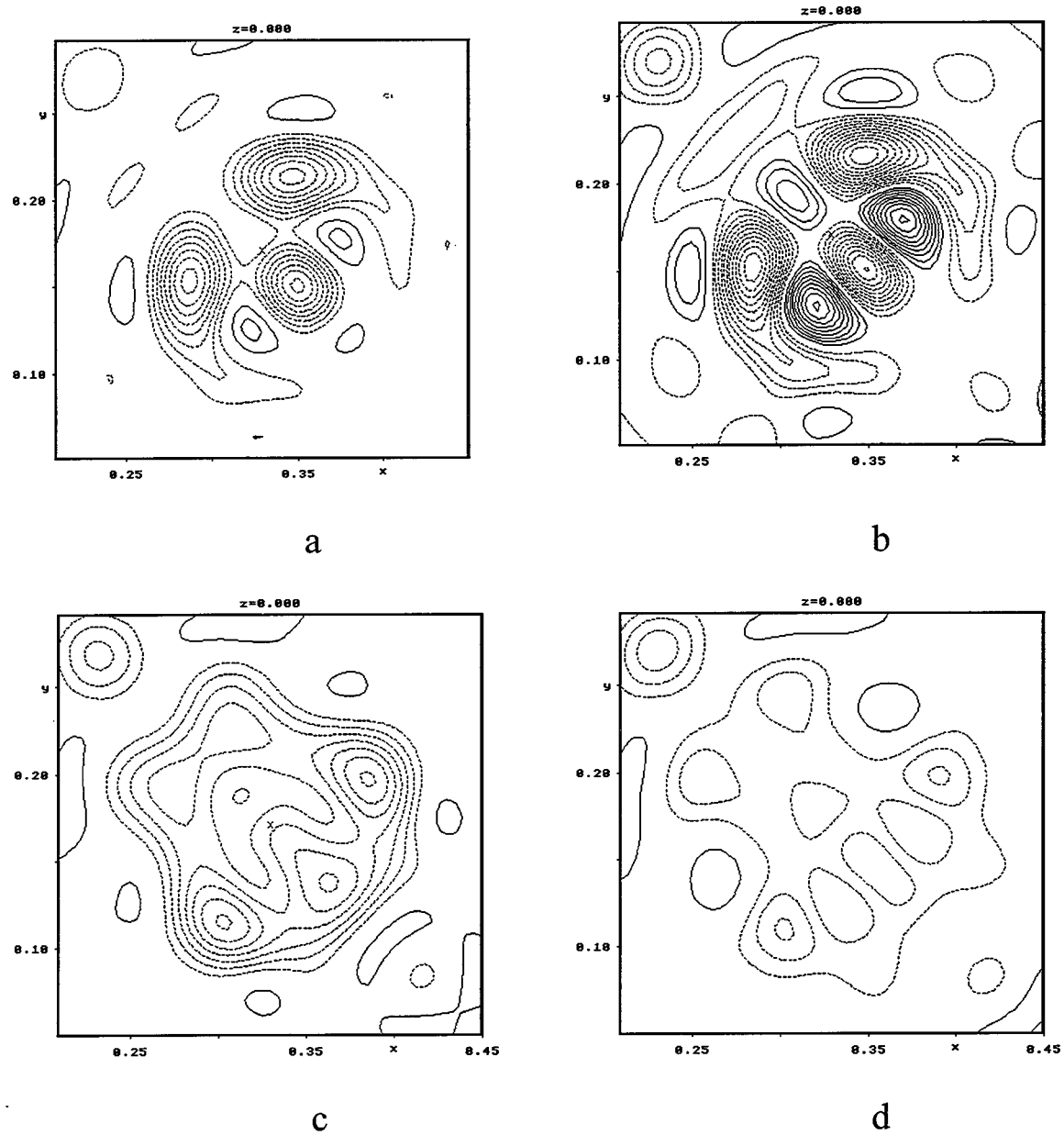


**FIG. 2.** Difference electron density map at $A(2)$ site (negative density is shown as dashed lines): (a) before occupancy and ADP refinement (contour interval at 0.5 e/Å$^3$); (b) after occupancy refinement (contour interval at 0.25 e/Å$^3$); (c) after ADP refinement (contour interval at 0.25 e/Å$^3$); (d) after occupancy and ADP refinement (contour interval at 0.25 e/Å$^3$).

apart or by anharmonic ADP of static origin. The latter approach is preferable because of the large correlation between atomic parameters of the split position.

The distributions of Ba and Ce between $A(1)$ and $A(2)$ sites were not known and could not be refined. Three extreme variants were refined: (i) both positions were refined as Ba, (ii) both positions were refined as Ce, and (iii) there was inverse distribution of Ba and Ce. In all cases the changes in occupancies were minor in comparison with the final results, while the changes in all other parameters (positional, ADP, occupational) were less than $\sigma$ if any. Taking into account the result of EDX analysis and final refinement we may state that both sites are occupied by both cations. Thus the influence of real occupation of these sites on the results of refinement is even smaller than in the cases mentioned above and the refinement of anharmonic displacement parameters is competent in this case.

The refinement of anharmonic ADP up to sixth order ($A(2)$ site occupancy was fixed to 1.0) gave $R = 0.021$ and $R_w = 0.024$ with 14 additional refinable parameters than in

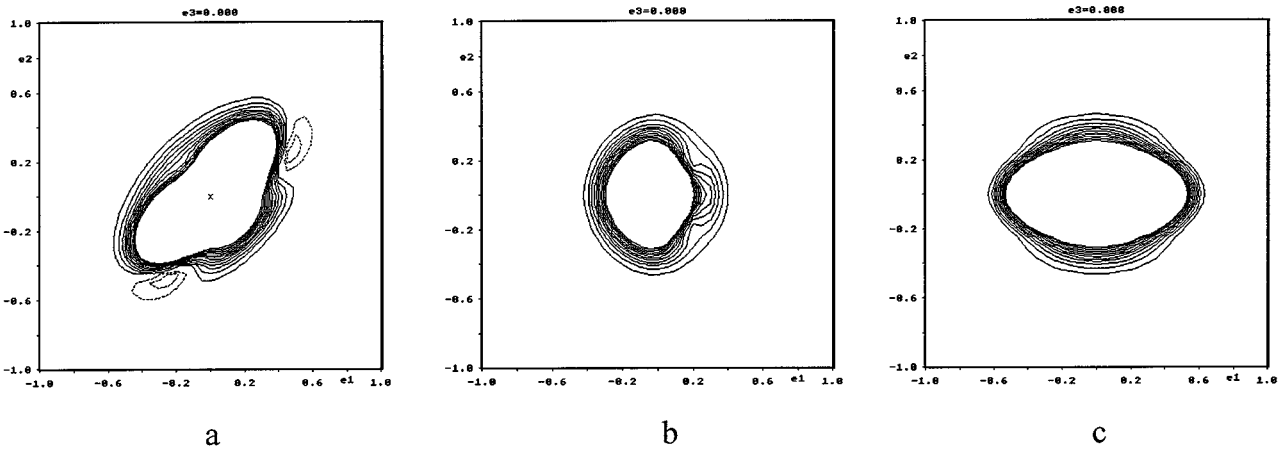


**FIG. 3.** Probability density function at $A(2)$ site: (a) $xy$ section; (b, c) sections perpendicular to $xy$ section; (b) parallel to $(1\bar{1}0)$ diagonal; (c) parallel to (110) diagonal.

the former case. The refinement resulted in five times reduction of the highest residual density, its smooth distribution over the studied area, and the absence of positive density regions (Fig. 2c). The distribution of $R$ factors over $\sin\theta/\lambda$ in this case was significantly different. In the latter case its variation was smaller, from 0.025 to 0.028 with minimal value $R = 0.017$ for $0.48 < \sin\theta/\lambda < 0.55$.[1] According to Hamilton test variations of $R$ factors in occupancy and ADP, refinements were significant; so at the final stage both $A(2)$ occupancy and its ADP were allowed to refine. The obtained composition, $(Ba, Ce)_{5.16(2)}Nb_{10}O_{30}$, is in agreement with the EDS analysis data.

The choice of the highest term for ADP refinement was done in the following way (12, 13). All symmetry-allowed harmonic terms up to sixth order were refined. All sixth order terms had a significance level of 0.33–1.5 $\sigma$. Taking into account high correlation coefficients ($> 0.9$) between some of the fourth- and sixth-order terms and the presence of pronounced negative regions in the probability density function (p.d.f.) map, these terms were withdrawn from refinement. For the fifth-order terms correlation coefficients were less and smaller in number (only one pair greater than 0.9), but the significance level of parameters was about the same as that in previous cases and the depth of the negative region was four times lower than that without the fifth-order terms. Thus in the final stage anharmonic ADP up to fourth order were refined.

Different sections of the p.d.f. at the $A(2)$ site are shown in Fig. 3. In general it looks like overlapping of at least three ellipsoids (two independent), which may result from the joint occupation of that site by two atoms different in size, namely Ba and Ce, about 0.2 Å apart. Thus an attempt was made to refine the $A(2)$ site as two separate sites for Ba and Ce with constrained anisotropic ADP. Oxygen atoms for which $U_{ii}$ were found to be very high (namely, $U_{11} = 0.076$ for O(3) and $U_{33} = 0.064$ for O(5)) were also refined in two sites. The same approach was used by Jamiesson and coworkers (1). The obtained $R$ factors were essentially the same as those in the case of the anharmonic ADP refinement. The refined sites were positioned 0.215 Å apart; the symmetry-related sites were 0.36 Å apart. Occupations of both sites are the same within standard deviations and equal to 0.30. Thus occupation of each site is too high for it to be occupied only by Ce.

Final $R$ factors are presented in Table 1; atomic positions, ADP, and selected interatomic distances are given in Tables 3, 4, 5, and 6. The refinement of the occupancies of the $A(1)$ and $A(2)$ sites showed that substitution of cerium for barium in $Ba_6Nb_{10}O_{30}$ led to the formation of the cation vacancies and consequently to the increase in the formal oxidation state of niobium. Moreover, the cation

**TABLE 3**
**Atomic Positions and ADP for $Ba_4CeNb_{10}O_{30}$**

| Atom | Site | Occupancy | $x$ | $y$ | $z$ | $U_{eq}$(Å) |
|---|---|---|---|---|---|---|
| $A(1)^a$ | 2*a* | 0.715(3) | 0 | 0 | 0 | 0.0082(1) |
| $A(2)^b$ | 4*g* | 0.934(3) | 0.32910(4) | $\frac{1}{2} - x$ | 0 | 0.0215(3) |
| Nb(1) | 2*c* | 1 | 0 | $\frac{1}{2}$ | $\frac{1}{2}$ | 0.0152(2) |
| Nb(2) | 8*j* | 1 | 0.07425(3) | 0.21250(3) | $\frac{1}{2}$ | 0.00853(10) |
| O(1) | 2*d* | 1 | 0 | $\frac{1}{2}$ | 0 | 0.0302(18) |
| O(2) | 4*h* | 1 | 0.2830(3) | $x + \frac{1}{2}$ | $\frac{1}{2}$ | 0.0135(10) |
| O(3) | 8*i* | 1 | 0.0743(5) | 0.2010(4) | 0 | 0.0390(17) |
| O(4) | 8*j* | 1 | −0.0065(3) | 0.3427(3) | $\frac{1}{2}$ | 0.0203(10) |
| O(5) | 8*j* | 1 | 0.1368(4) | 0.0674(3) | $\frac{1}{2}$ | 0.0331(15) |

[a] Refined as Ce site.
[b] Refined as Ba site.

[1] Eight $\sin\theta/\lambda$ intervals were chosen by the program with approximately equal numbers of reflections (77–99) in each.

**TABLE 4**
**Anitostropic ADP (Å$^2$) for $Ba_4CeNb_{10}O_{30}$**

| Atom | $U_{11}$ | $U_{22}$ | $U_{33}$ | $U_{12}$ |
|---|---|---|---|---|
| *A*(1) | 0.0077(2) | $U_{11}$ | 0.0093(3) | 0.0 |
| *A*(2) | 0.0253(5) | $U_{11}$ | 0.0138(6) | 0.0149(5) |
| Nb(1) | 0.0090(2) | $U_{11}$ | 0.0276(4) | −0.0016(3) |
| Nb(2) | 0.0071(2) | 0.0085(2) | 0.0099(2) | 0.00108(12) |
| O(1) | 0.041(3) | $U_{11}$ | 0.008(3) | −0.017(4) |
| O(2) | 0.0076(11) | $U_{11}$ | 0.025(3) | 0.0037(15) |
| O(3) | 0.076(4) | 0.036(3) | 0.0050(16) | −0.023(3) |
| O(4) | 0.0117(14) | 0.0066(12) | 0.043(2) | 0.0021(12) |
| O(5) | 0.025(2) | 0.0092(15) | 0.064(4) | 0.0126(14) |

**TABLE 6**
**Selected Interatomic Distances in $Ba_4CeNb_{10}O_{30}$**

| Atoms | Number | Distance | Atoms | Number | Distance |
|---|---|---|---|---|---|
| *A*(1)–O(3) | 4 | 2.681(5) | Nb(1)–O(1) | 2 | 1.9664(5) |
| *A*(1)–O(5) | 8 | 2.740(3) | Nb(1)–O(4) | 4 | 1.970(4) |
| *A*(2)–O(1) | 1 | 3.0233(5) | | | |
| *A*(2)–O(2) | 2 | 2.7926(16) | Nb(2)–O(2) | 1 | 1.992(2) |
| *A*(2)–O(3) | 2 | 3.209(6) | Nb(2)–O(3) | 2 | 1.9716(5) |
| *A*(2)–O(3′) | 2 | 3.460(6) | Nb(2)–O(4) | 1 | 1.916(3) |
| *A*(2)–O(4) | 4 | 2.850(3) | Nb(2)–O(5) | 1 | 2.009(4) |
| *A*(2)–O(5) | 4 | 3.366(4) | Nb(2)–O(5′) | 1 | 1.978(4) |

vacancies are preferably localized in the *A*(1) site with a cuboctahedral coordination of oxygen atoms. This result is in agreement with previous studies of compounds with a TTB-type structure. For example, in $K_{0.37}WO_3$, the occupancies of the *A*(1) and *A*(2) sites are, respectively, 0.105 and 0.875 (14).

The partial replacement of Ba atoms by Ce ones and creation of cation vacancies in the *A*(1) sites led to a decrease in the effective ionic radius of the *A*(1) cations. This resulted in significant shortening of the *A*(1)–O(5) and especially *A*(1)–O(3) interatomic distances and therefore in the distortion of $A(1)O_{12}$ cuboctahendron in comparison with the $Ba_6Nb_{10}O_{30}$ structure. At the same time, the *A*(2) polyhedron remains essentially unaffected. Just a small ($\sim$ 0.010–0.020 Å) decrease in the *A*(2)–O interatomic distances was observed. These data confirmed our suggestion about preferable occupation of *A*(1) sites by smaller Ce atoms while Ba atoms are located mainly in the *A*(2) sites.

The $Nb(1)O_6$ octahedron is almost regular while Nb(2)–O interatomic distances differ considerably (1.916–2.009 Å). The main distinction from the $Ba_6Nb_{10}O_{30}$ structure is a shortening of the Nb(2)–O(5′) and Nb(2)–O(4) distances. The other Nb–O bonds remain essentially unchanged. The average Nb(1)–O and Nb(2)–O interatomic distances are slightly smaller than those in the $Ba_6Nb_{10}O_{30}$ structure.

**TABLE 5**
**Anharmonic ADP of *A*(2) Site ($C_{ijk}\times10^3$, $D_{ijkl}\times10^4$) in $Ba_4CeNb_{10}O_{30}$**

| | |
|---|---|
| $C_{111} = 0.00059(6)$ | $D_{1111} = -0.00012(4)$ |
| $C_{112} = 0.00024(3)$ | $D_{1112} = -0.00014(2)$ |
| $C_{122} = -C_{112}$ | $D_{1122} = -0.00011(2)$ |
| $C_{133} = -0.0006(3)$ | $D_{1133} = -0.00004(13)$ |
| $C_{222} = -C_{111}$ | $D_{1222} = D_{1112}$ |
| $C_{233} = -C_{133}$ | $D_{1233} = -0.00021(13)$ |
| | $D_{2222} = D_{1111}$ |
| | $D_{2233} = D_{1133}$ |
| | $D_{3333} = 0.008(5)$ |

The relative size and orientation of displacement ellipsoids are shown in Fig. 4. Short distances from *A*(2) to O(2) and O(4) do not allow any shift in the direction of these bonds, neither for *A*(2) nor for O(2) and O(4). Large *A*(2)–O(1) and especially *A*(2)–O(3) distances allow these atoms to be located in a rather wide region. The same is true for the O(5) atom, with a distance to *A*(2) that exceeds 3.3 Å, and the displacement ellipsoid of O(5) is oriented toward the *A*(1) site ($d_{A(1)\text{-}O(5)} = 2.740(3)$ Å). A large number of vacancies in the *A*(1) site gives additional freedom for exact positioning of O(5) in each particular unit cell.

The displacement ellipsoids of O(3) are oriented perpendicular to the shortest *A*(1)–O bond in the structure ($d_{A(1)\text{-}O(3)} = 2.681(5)$ Å). The orientation of the O(1) displacement ellipsoid is determined by the presence of the empty C channels in the structure. Thus the shift of O(1) to the empty C channels is maximal. This in turn leads to the high $U_{33}$ for the Nb(1) atoms for which the O(1) atoms are axial and therefore to the high $U_{33}$ for the equatorial O(4) atoms. This all together reflects the shift of the $Nb(1)O_6$ octahedra along the *z* axis ($U_{33}$ for Nb1 is high and is likely to reflect static disorder rather than thermal vibration). The behavior of the Nb(2) atom is different from that of the Nb(1) atom. All $U_{ij}$ for Nb(2) are about the same order of magnitude and are small; so it is more likely that this octahedron is tilted, as was described by Jamiesson *et al.* (1). This is probably due to the fact that the displacements of the surrounding oxygen atoms are in different directions. As was mentioned above the displacements of the equatorial O(2) and O(4) oxygen atoms are determined by the short *A*(2)–O(2) and *A*(2)–O(4) distances while those of the O(3) and O(5) atoms are determined by the short *A*(1)–O(3) and *A*(1)–O(5) distances (Table 6).

The result of the single crystal refinement of the reduced niobate with a TTB-type structure confirms that heterovalent substitution of $Ce^{3+}$ for $Ba^{2+}$ can lead to the formation of cation vacancies in the *A* sites. The concentration of the vacancies in the smaller *A*(1) cavities is larger than that in the larger *A*(2) cavities. However, formation of vacancies in the *A* site is not accompanied by creation of oxygen

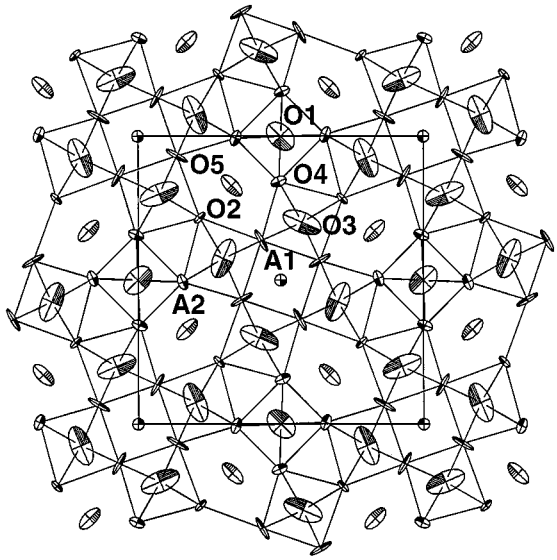


**FIG. 4.** The crystal structure of $Ba_4CeNb_{10}O_{30}$.

vacancies in the structure. This leads to an increase in the formal oxidation state of niobium. According to elemental analysis, the formal oxidation state of niobium was $+4.9$ compared with $+4.6$ for the $Ba_4Ce_2Nb_{10}O_{30}$ composition with fully occupied *A* positions. BVS calculations showed the average oxidation state of niobium to be close to $+5$. These data confirm the results of Rietveld analysis on powder samples of $Ba_{6-x}Ln_xNb_{10}O_{30}$, $Ln$ = La, Ce, and Nd (7). Therefore nonmetallic behavior of reduced niobates with TTB-type structure can be explained by low charge carrier concentrations. To prepare more reduced compounds with TTB-type structure synthetic conditions suppressing the formation of cation vacancies (for example, high pressure–high temperature technique) can be used.

## ACKNOWLEDGMENTS

We are grateful to Dr. K. Kalmikov for EDS analysis. This work has been supported by the Russian Foundation for Basic research (Grant 97-03-33432a).

## REFERENCES

1. P. B. Jamiesson, S. C. Abrahams, and J. L. Bernstein, *J. Chem. Phys.* **48,** 5048 (1968).
2. P. B. Jamiesson, S. C. Abrahams, and J. L. Bernstein, *J. Chem. Phys.* **54,** 2355 (1971).
3. N. Kumada and N. Kinomura, *Eur. J. Solid State Inorg. Chem.* **34,** 65 (1997).
4. B. Hessen, S. A. Sunshine, T. Siegrist, and R. Jimenez, *Mater. Res. Bull.* **26,** 85 (1991).
5. B. Hessen, S. A. Sunshine, T. Siegrist, A. Fiory, and J. Waszak, *Chem. Mater.* **3,** 528 (1991).
6. Y. K. Hwang and Y.-U. Kwon, *Mater. Res. Bull.* **32,** 1495 (1997).
7. O. G. D'yachenko, S. Ya. Istomin, M. M. Fedotov, E. V. Antipov, G. Svensson, M. Nygren, and W. Holm, *Mater. Res. Bull.* **32,** 409 (1997).
8. L. Muhlenstein and G. Danielson, *Phys. Rev.* **158,** 825 (1967).
9. C. R. Feger and R. P. Ziebarth, *Chem. Mater.* **7,** 373 (1995).
10. V. Petricek and M. Dusek, "JANA98 Manual," 1998.
11. A. E. Andreychuk, L. M. Dorozhkin, Yu. S. Kuz'minov, I. A. Maslyanicyn, V. N. Molchanov, A. A. Russakov, V. I. Simanov, V. D. Shigorin, and G. P. Shipulo, *Kristallografiya* (*Rus.*) **29,** 1094 (1986).
12. W. F. Kuhs, *Acta Crystallogr. A* **39,** 148 (1983).
13. W. F. Kuhs, *Acta Crystallogr. A* **48,** 80 (1992).
14. L. Kihlborg and A. Klug, *Chem. Scr.* **3,** 207 (1973).